2024 IEEE/RSJ International Conference on Intelligent Robots and Systems (IROS)
October 14-18, 2024. Abu Dhabi, UAE

Modeling and Gait Analysis of Passive Rimless Wheel with Compliant Feet

Yanqiu Zheng[1], Cong Yan[1], Yuetong He[2], Fumihiko Asano[2] and Isao T. Tokuda[1]

***Abstract*— The movement of the legs involves the interaction between the feet and the ground. Consequently, most animals possess a wide variety of foot morphologies and multifunctional capabilities. The selection and switching of these foot functions are passive and environment-dependent, ensuring environmental compliance. Despite this, current research on compliant feet lacks mathematical models that simultaneously encompass locomotion and foot compliance. Therefore, conducting in-depth studies on locomotion properties under current conditions is challenging. In this study, we present novel passive compliant feet applicable to the passive walking of a rimless wheel. We first introduce a dynamic model, achieve passive walking through numerical simulations, and subsequently analyze the gait patterns for compliance and multi-period gait. This study bridges a gap in understanding the interaction between motion and compliance in foot design, providing insights into the dynamics of compliant motion.**

I. INTRODUCTION

Legged locomotion enables animals to navigate diverse terrains with a high degree of agility, obstacle avoidance, and other capabilities that cannot be matched by other forms of motion [1]–[3]. The fundamental element of this motion is the interaction between the legs and ground, and one of the basic mechanisms by which stability, propulsion, and adaptability are provided is through the feet [4].The morphology of animal feet is incredibly diverse, a testament to the myriad ways that form has evolved to meet specific locomotor needs and ecological habitats [5]. From the padded paws of felines to the webbed feet of aquatic birds, the diversity that characterizes the structure of animal feet has been optimized for efficient locomotion and adaptation to their environments.

Passive compliance [6] emerges as a principal mechanism through which animals adjust their mechanics. Unlike active systems, which depend on continuous energy input, passive compliance allows biological constructs to change their form in response to external stimulation or environmental changes, without necessitating conscious control [7]. This inherent adaptability allows animal feet to adjust their behavior dynamically as a function of terrain stiffness, slope, and irregularities, thereby optimizing locomotion robustness and efficiency [8], [9]. By passively adapting to the terrain, the animals' feet can minimize energy consumption while maximizing grip or stability, thus enabling flexible locomotion in a variety of environments [10], [11]. As shown in Fig. 1 (a), the feet of geckos have a number of small and fine capillary structures which can produce intermolecular adsorption force, known as van der Waals force, at a microscopic level. The two modes of rapid sticking and peeling from surfaces are not active choices by geckos, but rather represent passive gait-based adaptation [12]. Fig. 1 (b) shows the silent walking or high-speed running exhibited by cheetahs passively, due to their curved claws which can extend to hook onto surfaces or retract according to different environments [13].

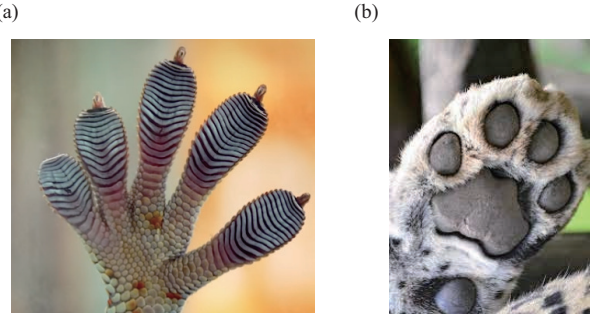

Fig. 1. Animal's multifunctional feet, (a) the claws of the gecko, have tiny hairs that can create an adsorption force, but will not always adsorb to the contact surface, and will adhere to or leave the contact surface passively while moving. (b) the cheetah's claws, which can reach out and grasp the ground when running at high speeds or retract their claws to achieve stealth moving.

Although the importance of compliant foot structures in promoting efficient movement over different terrains has been well recognized [14]–[16], current research efforts suffer from an insufficiency: a shortage of content that combines dynamic legged locomotion and compliant feet to investigate the effects of walking gait. While numerous studies have investigated the biomechanics of leg movement or the compliance of individual foot structures, there is still a lack of a coherent framework that brings these two aspects together into a unified understanding, hampering understanding of how compliant feet improve overall movement. This research gap limits our ability to fully understand the intricate interplay between foot morphology, compliance, and dynamic legged locomotion to better exploit the structural properties of the system, making movement control costly and inefficient.

This research was partially supported by Grant–in–Aid for Research Activity Start-up No. 23K19101, provided by the Japan Society for the Promotion of Science (JSPS). The author from Ritsumeikan University who participates in this IROS conference was partially supported by the IROS Development and Promotion Fund.

[1]Yanqiu Zheng, Cong Yan and Isao T. Tokuda are with the Department of Mechanical Engineering, Ritsumeikan University, 1-1-1 Nojihigashi, Kusatsu Shiga 525-8577, Japan {zhengyq, gansou, isao}@fc.ritsumei.ac.jp

[2]Fumihiko Asano is with the Graduate School of Advanced Science and Technology, Japan Advanced Institute of Science and Technology, 1-1 Asahidai, Nomi, Ishikawa 923-1292, Japan. {s2220012, fasano}@jaist.ac.jp

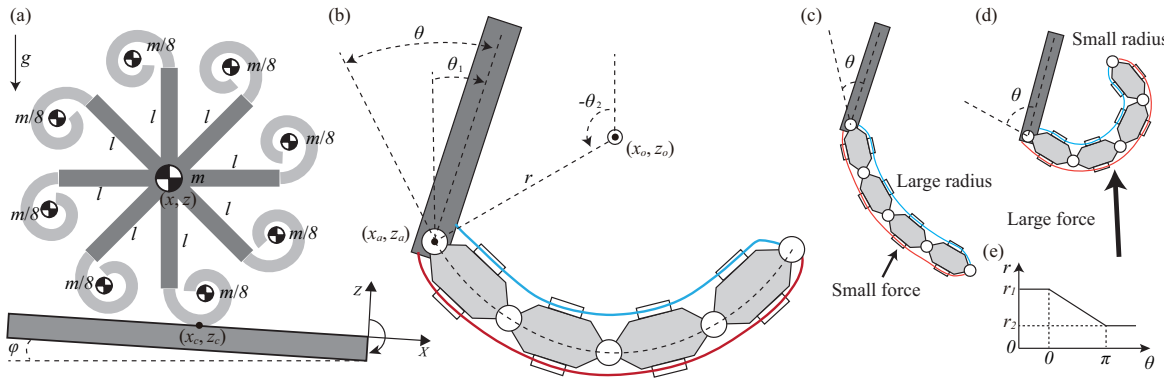

Fig. 2. Proposed mathematical passive rimless wheel model with compliant feet. Here, (a) is a mathematical model diagram in which the radius of the compliant feet r [m] changes while walking, (b) is a detailed diagram of a foot that can change r through elastic lines based on the ankle angle θ [rad], and (c)(d) represents how the r and θ adjust when the foot experiences various external forces, predominantly the ground support forces. Additionally, (e) illustrates the linear relationship between r and θ as established in this study.

As a representative model of legged locomotion, the rimless wheel [17], [18] has a simple structure, which can represent the continuous and discrete processes of legged locomotion. Passive walking [19] has been proven to be the most similar to human walking, not only efficient but also making great use of the dynamic characteristics of its structure. Therefore, the passive gait based on the rimless wheel has revealed a large amount of relevant theories on human gait. In this context, the arc feet [20] have been proven to cushion the impact with the ground, providing higher walking speed during movement. Most importantly, they can map biological processes such as the entire motion process from foot contact to rolling like the human feet.

Therefore, in this study, we propose compliant arc feet with variable radii attached to the rimless wheel. In passive walking, the foot radii are adjusted based on the angle between the foot and the leg, allowing the foot shapes to conform to the leg movement, adapting to factors such as ground reaction forces in an adaptive gait. This study serves as an extension of the rimless wheel model, with the variable-radius compliant foot as the research target, filling the gap in its flexible motion. Therefore, this study can be seen as a landmark in expanding the rigid-body rimless wheel model to achieve flexible motion.

The present paper is organized as follows. In Section II, we delineate the model design and dynamic modeling, focusing on constraint forces, compliance force calculations, and collision equations. Section III begins with a numerical simulation showcasing both period-1 and period-2 gaits. Subsequently, an analysis of how various compliance factors affect gait across diverse environments is presented. The final section is devoted to general discussions on the applications of the present model in legged locomotion and its implications for biology.

II. MODEL DESIGN AND MATHEMATICAL METHODS

Fig. 2 (a) illustrates a passive walking model of the rimless wheel with 8 compliant feet, while Fig. 2 (b) provides a detailed description of it. As depicted in Fig. 2 (b), a foot consists of multiple joints, forming a flexible structure similar to human fingers. On either side, there are red and blue elastic cables as depicted in the figure. These elastic cables, with different natural lengths, contribute to the foot maintaining a stable curved shape. Therefore, as illustrated in Fig. 2 (c,d), when an external force is applied to the foot, it disrupts the current force equilibrium and results in a new stable shape. Specifically, a small external force causes a larger curvature of the foot, while a large external force has the opposite effect. The relationship between the radius of the foot and the angle of the ankle is shown in Fig. 2 (e). Consequently, this structure provides the foot with shape compliance, enabling it to change its shape to adapt to the environment while walking.

In the model, the radius of the rimless wheel is l [m] and its mass is m [kg], while the radius of the foot is r [m] and its mass is $m/8$ [kg]. The center position of the rimless wheel is (x,z), and the angle between the vertical direction is θ_1 [rad]. The position of the ankle is (x_a,z_a), and the center position of the foot is (x_o,z_o), while θ_2 [rad] is the angle of the foot to the vertical direction. The slope angle is ϕ [rad] and the point of contact with the ground is defined as $(x_c.z_c)$.

A. Equation of Motion and Holonomic Constraints

Let $\boldsymbol{q} = \begin{bmatrix} x & z & \theta_1 & \theta_2 \end{bmatrix}^{\mathrm{T}}$ be the generalized coordinate vector, then the equation of motion is

$$\boldsymbol{M}\ddot{\boldsymbol{q}} + \boldsymbol{h} = \boldsymbol{J}^{\mathrm{T}}\boldsymbol{\lambda} + \boldsymbol{S}u, \tag{1}$$

where $\boldsymbol{M}$ is the inertia matrix, $\boldsymbol{h}$ represents the combination of central force, Coriolis accelerations, and gravity terms. On the right-hand side, $\boldsymbol{J}$ is the Jacobian matrix for the holonomic constraints at the grounding point (x_c,z_c), and $\boldsymbol{\lambda}$ is the vector of constraint forces. $\boldsymbol{S}u$ is the internal compliance that affects the shape of the foot.

According to the geometric relationship shown in Fig. 2 (b), the coordinates of the ankle can be obtained as

$$\begin{bmatrix} x_a \\ z_a \end{bmatrix} = \begin{bmatrix} x - l\sin\theta_1 \\ z - l\cos\theta_1 \end{bmatrix}, \tag{2}$$

in addition, the positional relationship between the ankle and the foot is

$$\begin{bmatrix} x_a \\ z_a \end{bmatrix} = \begin{bmatrix} x_o + r\sin\theta_2 \\ z_o + r\cos\theta_2 \end{bmatrix}. \tag{3}$$

Consequently, the attitude of the robot can be determined by θ_1 and θ_2. The compliance of the foot is determined by its radius, r [m]. When the foot is subjected to an external force, it changes the ankle angle, θ [rad]. Therefore, the radius of the foot has a certain functional relationship with the ankle angle. Here, the function we utilized is shown below and the shape is demonstrated in Fig. 2 (e).

$$r = \begin{cases} r_1 + \frac{r_2 - r_1}{\pi}\theta & 0 < \theta \leq \pi \\ r_1 & \theta \leq 0 \\ r_2 & \theta > \pi \end{cases}, \tag{4}$$

where r_1 [m] is the upper limit of the set radius and r_2 [m] is the lower limit of it. The angle of ankle θ [rad] between leg and foot can be obtained as

$$\theta = \theta_1 - \theta_2 - \pi/2. \tag{5}$$

In reality, r is based on the equilibrium of elastic and reaction forces and is therefore more complex and nonlinear, here we use a linear function to approximate this behavior to simplify the calculation.

According to Eq. 3 and Eq. 4, the center and radius of the foot can be obtained, then the lowest point of the foot can be considered as the point of contact with the ground as

$$\begin{bmatrix} x_c \\ z_c \end{bmatrix} = \begin{bmatrix} x_o + r\sin\theta_2 \\ z_o + r\cos\theta_2 \end{bmatrix}_{\theta_2=\pi}. \tag{6}$$

By differentiating it, we can get

$$\begin{bmatrix} \dot{x_c} \\ \dot{z_c} \end{bmatrix} = \begin{bmatrix} \dot{x_o} + \dot{r}\sin\theta_2 + r\cos\theta_2\dot{\theta_2} \\ \dot{z_o} + \dot{r}\cos\theta_2 - r\sin\theta_2\dot{\theta_2} \end{bmatrix}_{\theta_2=\pi} = \begin{bmatrix} \dot{x_o} - r\dot{\theta_2} \\ \dot{z_o} - \dot{r} \end{bmatrix}. \tag{7}$$

Then the Jacobian matrix $\boldsymbol{J}$ of the grounding point can be obtained by the following equation.

$$\begin{bmatrix} \dot{x_c} \\ \dot{z_c} \end{bmatrix} = \boldsymbol{J}\dot{\boldsymbol{q}}. \tag{8}$$

In walking, we use the rolling without slipping assumption, therefore the constraint conditions at the grounding point can be assumed as

$$\begin{bmatrix} \dot{x_c} \\ \dot{z_c} \end{bmatrix} = \begin{bmatrix} 0 \\ 0 \end{bmatrix}. \tag{9}$$

By differentiating it, we can get constraints on $\ddot{\boldsymbol{q}}$ as

$$\begin{bmatrix} 0 \\ 0 \end{bmatrix} = \dot{\boldsymbol{J}}\dot{\boldsymbol{q}} + \boldsymbol{J}\ddot{\boldsymbol{q}}. \tag{10}$$

Then, by solving Eq. (1) with Eq. (10) simultaneously, the constraint force vector $\boldsymbol{\lambda}$ can be derived as

$$\boldsymbol{\lambda} = -\boldsymbol{X}^{-1}\boldsymbol{J}\boldsymbol{M}^{-1}(\boldsymbol{S}u - \boldsymbol{h}) + \dot{\boldsymbol{J}}\dot{\boldsymbol{q}}, \tag{11}$$

where $\boldsymbol{X} := \boldsymbol{J}\boldsymbol{M}^{-1}\boldsymbol{J}^{\mathrm{T}}$.

B. Internal Compliance

Eq. (4) shows the mapping relationship of the adaptive shape of the foot, where r and θ are both functions of $\theta_1 - \theta_2$. Therefore, the essence of its compliance torque u [N/m] is actually acting on the ankle. Based on this, we define the control matrix $\boldsymbol{S}$ as

$$\boldsymbol{S} = \begin{bmatrix} 0 & 0 & 1 & -1 \end{bmatrix}^{\mathrm{T}}. \tag{12}$$

Here, 1 and -1 in $\boldsymbol{S}$ represent the action and reaction forces of $\boldsymbol{u}$, without implying any specific magnitudes. The radius of the foot is ultimately affected by the compliance torque, hence setting the actuation target $y = r$, then its differential can be written as follows:

$$\dot{y} = \dot{r} = \boldsymbol{J}_c\dot{\boldsymbol{q}}, \tag{13}$$

where $\boldsymbol{J}_c$ is the Jacobian matrix for mapping generalized coordinates to the actuation target. Given $\boldsymbol{J}_c$ equals $\boldsymbol{S}$, it proves that the target can be actuated by compliance torque u [N·m].

Accordingly, we utilize the following spring damping system to guarantee the soft characteristics and compliance of the foot:

$$u = -k(r_d - r) - c(0 - \dot{r}), \tag{14}$$

where k [N/m] and c [N·s/m] are coefficients of elasticity and viscosity respectively. r_d [m] is the designed radius, which is also the target for stabilization.

C. Collision Equation

Since it can be considered as an inelastic collision. Thus, based on angular momentum conservation, the collision equation is presented as follows.

$$\boldsymbol{M}\dot{\boldsymbol{q}}^{+} = \boldsymbol{M}\dot{\boldsymbol{q}}^{-} + \boldsymbol{J}_I^{\mathrm{T}}\boldsymbol{\lambda}_I, \tag{15}$$

$$\boldsymbol{J}_I\dot{\boldsymbol{q}}^{+} = \begin{bmatrix} 0 \\ 0 \end{bmatrix}, \tag{16}$$

where $\boldsymbol{J}_I$ is the Jacobian matrix of the collision position, which indicates an angular impulse changing the total angular momentum at the swing leg (collision leg). Meanwhile the superscripts "$-$" and "$+$" denote the instances immediately before and after this collision, respectively.

The angle of the collision leg is $\theta_1 - \alpha$ [rad], where $\alpha := 2\pi/8$ [rad] is the angle between each leg and r_d [m] based on Eq. 14 corresponds to the designed radius. Then the designed angle of the collision foot can be calculated as θ_{2d} [rad], thus $\boldsymbol{J}_I$ can be obtained as

$$\boldsymbol{J}_I(\theta_1, \theta_2) = \boldsymbol{J}(\theta_1 - \alpha, \theta_{2d}), \tag{17}$$

where

$$\theta_{2d} = \theta_1 - \alpha - \pi/2 - (r_d - r_1)/((r_2 - r_1)/\pi) \tag{18}$$

corresponds to the designed radius r_d [m] of the collision foot according to Eq. 4 and Eq. 5.

By solving Eqs. (15) and (16) simultaneously, the velocities of generalized coordinates after collision $\dot{\boldsymbol{q}}^{+}$ can be obtained as

$$\dot{\boldsymbol{q}}^{+} = \left(\boldsymbol{I}_4 - \boldsymbol{M}^{-1}\boldsymbol{J}_I^{\mathrm{T}}\boldsymbol{X}_I^{-1}\boldsymbol{J}_I\right)\dot{\boldsymbol{q}}^{-}, \tag{19}$$

where $\boldsymbol{X}_I := \boldsymbol{J}_I\boldsymbol{M}^{-1}\boldsymbol{J}_I^{\mathrm{T}}$.

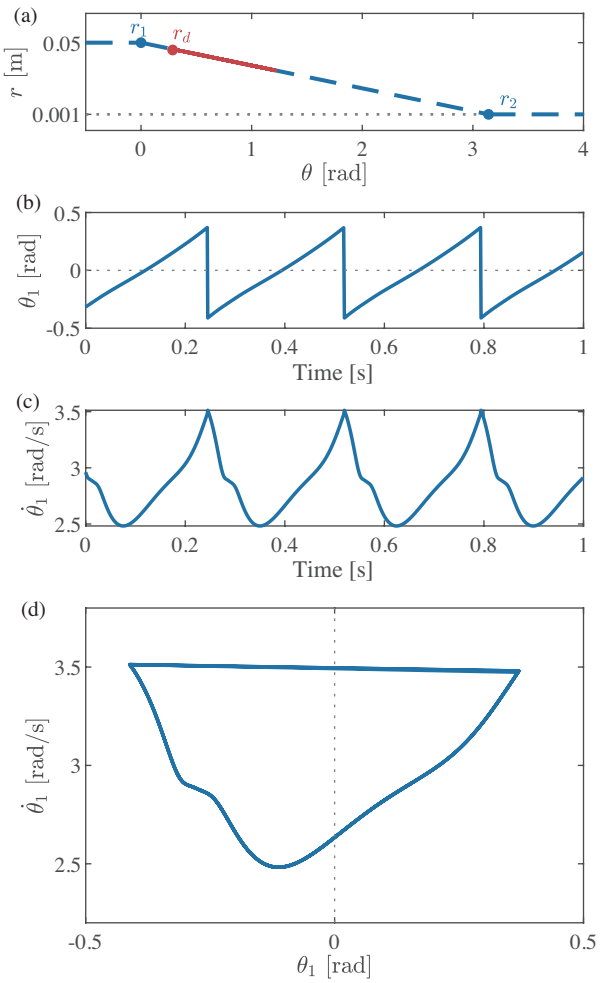

Fig. 3. Simulation results for period-1 gait: (a) features a diagram mapping ankle angle to foot radius. (b) and (c) show plots of leg angular position and velocity over time, while (d) include plots of their respective phases.

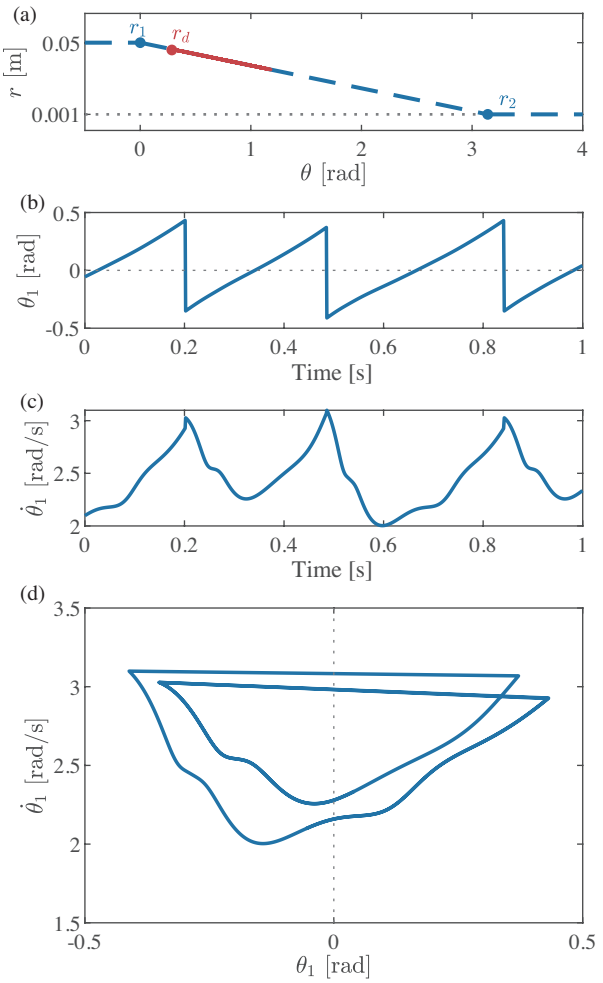

Fig. 4. Simulation results for period-2 gait: (a) features a diagram mapping ankle angle to foot radius. (b) and (c) show plots of leg angular position and velocity over time, while (d) include plots of their respective phases.

III. NUMERICAL SIMULATION EXPERIMENT

Numerical simulation experiments were conducted using 'MATLAB R2023b' as the simulation software. The 'ode45' function in MATLAB was employed to solve the differential equations of the motion equations. The step size was set to 0.001 [s], and relative and absolute tolerances were set to '1e-6' to ensure simulation accuracy. Specific physical parameters and control parameter settings are presented in Table I.

TABLE I
PARAMETER SETTINGS

Symbol	Value	Unit
m	2	kg
l	0.25	m
r_1	0.05	m
r_2	0.001	m
r_d	0.045	m
k	500	N/m
c	5	N·s/m

A. Gait Generation

When the slope is set to 0.18 [rad], a typical period-1 limit gait as shown in Fig. 3 is generated. We choose the initial state to be with double-legged support on the ground, and the stance leg with a relatively high initial kinetic energy ($\dot{\theta}_1(0) = 5$ [rad/s]) to ensure that the robot could overcome the initial potential energy barrier. Data from 20 [s] into the simulation are selected to ensure gait convergence and data stability. Based on Eq. 14 and the set radius r_d, we can obtain the corresponding elastic force, which can be used to counteract the environmental reaction force, thereby ensuring stable locomotion.

Fig. 3 (a) represents the relationship between ankle angle and foot radius during motion, where the blue dashed line represents the set linear mapping determined by r_1 [m] and r_2 [m], and the solid red line represents the actual range of variation when the radius is set to r_d [m]. Firstly, it can be noted that the actual mapping strictly follows the set trajectory, which is crucial for achieving foot shape compliance. Secondly, although the radius is set to r_d [m], the actual motion does not stabilize precisely at r_d [m] but

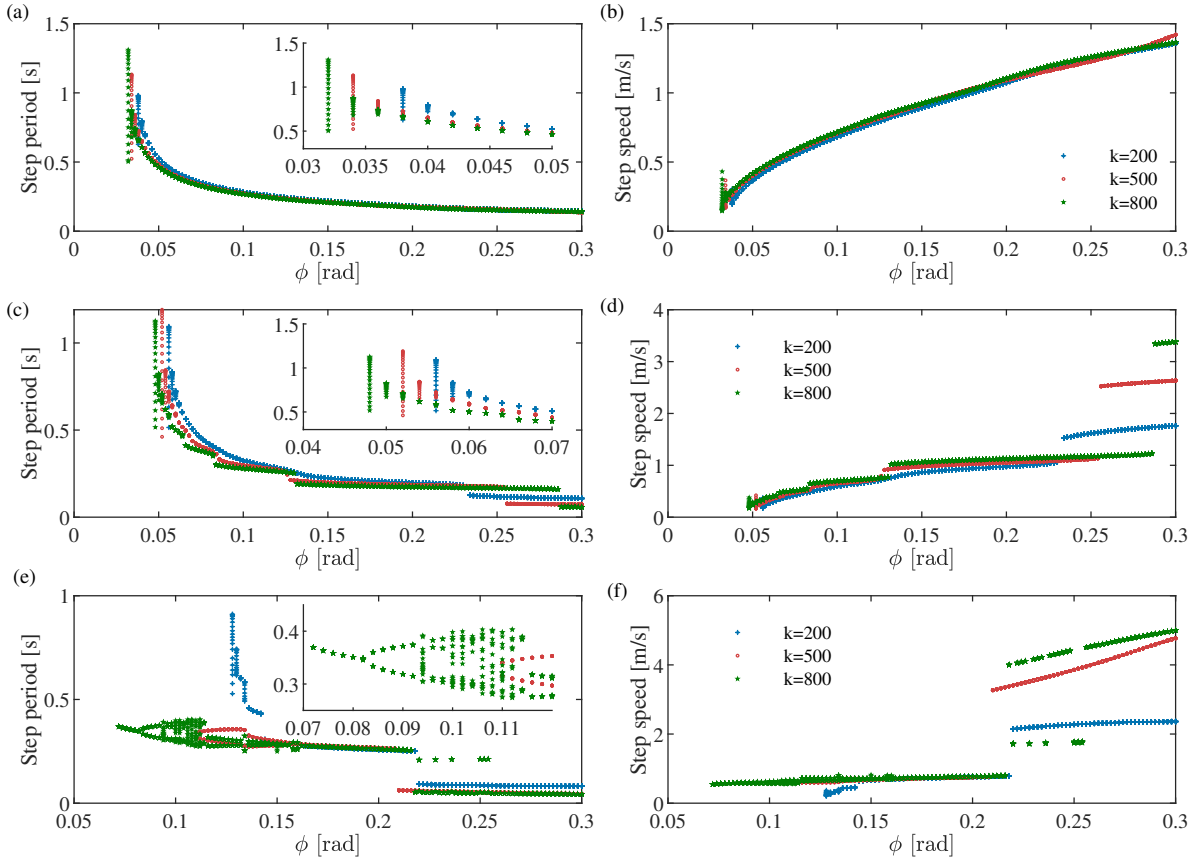

Fig. 5. Walking gait corresponds to the increasing slope of different targets radius r_d [m]. (a) and (b) depict the step period and step speed for $r_d = 0.025$ [m]. (c) and (d) illustrate the step period and step speed for $r_d = 0.035$ [m]. Lastly, (e) and (f) is the step period and step speed for $r_d = 0.045$ [m].

rather exhibits a range due to the compliant force of the spring-damper system, resulting in oscillations. Additionally, since the foot is continuously subjected to an upward force while walking from the ground, the radius variation will yield a range smaller than r_d [m]. Fig. 3 (b) and (c) display the angular positions, and angular velocities of the legs, while Fig. 3 (d) illustrates their phase diagram. It can be observed that the gait exhibits periodic motion at this stage, with each step maintaining the same motion state, as shown by the period-1 limit cycle depicted in Fig. 3 (d).

When the slope is reduced to 0.13 [rad], however, a period-2 gait, as shown in Fig. 4, emerges. Contrasting all figures with Fig. 3, the key difference lies in the consistent movement state every two steps. This indicates that the slope has a significant impact on compliant gaits. In passive walking, the slope represents external input energy, whereas a larger slope implies greater external energy. Therefore, it can be observed that larger external energy can induce compliant gaits to converge to stability, whereas smaller external energy cannot fully suppress the dynamic characteristics of gaits , leading to multi-periodic phenomena.

B. Compliance Characteristics

Fig. 5 illustrates the step period and step speed for different control objectives, represented by r_d [m]. Fig. 5 (a) and (b) depict the results for r_d set to 0.025 [m], Fig. 5 (c) and (d) for r_d set to 0.035 [m], and Fig. 5 (e) and (f) for r_d set to 0.045 [m]. When r_d is set to 0.025 [m], it can be observed that as the slope increases, indicating an increase in external energy, the gait tends towards stability. On the other hand, varying k [N/m], representing different degrees of foot compliance, yields almost identical gaits, indicating that the stiffness of the foot has little effect on the gait. This is because the small value of r_d minimizes the influence of foot compliance on the gait. Increasing r_d to 0.035 [m], however, Fig. 5 (c) shows that at high slopes (greater than 0.25 [rad]), discontinuities occur, which become more pronounced at the corresponding position in Fig. 5 (d), where the speed increases. Moreover, smaller values of k lead to earlier occurrences of this phenomenon. As r_d continues to increase, Fig. 5 (e) and (f) demonstrate that the discontinuities at high slopes become more pronounced, with higher speeds. Additionally, nonlinear phenomena become stronger at low slopes, and bifurcation phenomena become more apparent.

C. Essence of Multi-periodic Gait

The presence of a compliant foot leads to the occurrence of multi-periodic nonlinear phenomena in the system. We presume that the motion of the compliant foot radius r and the motion of the robot's legs θ_1 are influenced by a nonlinear mapping relationship. As the robot walks, it encounters

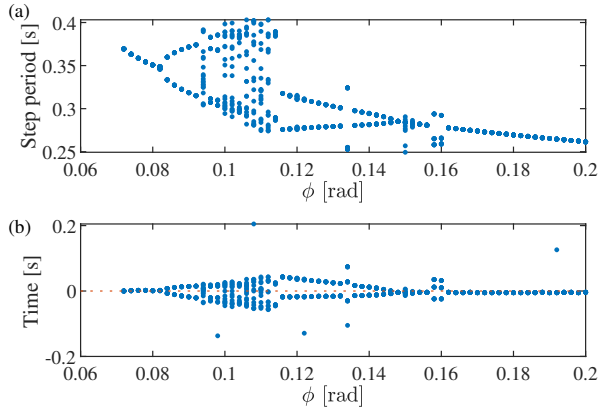

Fig. 6. Bifurcation diagram for walking. (a) is a replication based on Fig. 5 (e), and (b) represents the time difference between the peak radius moment and the peak potential energy moment calculated for (a).

potential energy barriers, with the maximum potential energy barrier position for the rimless wheel occurring at θ_1 equal to 0. Therefore, we recorded the corresponding time t_1 when θ_1 is 0 for each walking period and also recorded the time t_2 corresponding to the maximum value of r within one period. Hence, the difference between t_1 and t_2 can be considered as the motion difference between the foot radius and the leg motion. Fig. 6 (a) is a replication based on Fig. 5 (e), $k = 800$ [N/m], because it exhibits typical nonlinear features such as single-cycle, multi-cycle, bifurcation, and chaotic phenomena, while Fig. 6 (b) presents the results based on $t_1 - t_2$. It can be observed that when a period-1 gait occurs, $t_1 - t_2$ almost approaches 0, indicating that their relationship satisfies the following equation:

$$\mathrm{Max}(r + (-|\theta_1|)) = \mathrm{Max}(r) + \mathrm{Max}(-|\theta_1|), \qquad (20)$$

where r [m] can be represented as the motion of the compliant part, while $-|\theta_1|$ [rad] can be represented as the potential energy barrier part.

This indicates that if the resonant motion occurs between the compliant part and the torso, it will reflect the motion characteristics of the torso; otherwise, it will reflect the motion characteristics corresponding to the compliant part.

IV. CONCLUSIONS

This study proposes a new model based on the rimless wheel model to simulate the compliance of the foot, enabling it to adapt its shape to ground reaction forces during walking. By providing a dynamic model and conducting simulations, we discovered the existence of single-cycle and multi-cycle gaits. Furthermore, we investigated the influence of compliance characteristics on gait and provided a fundamental explanation for the generation of single-cycle gait.

Through this study, we have gained a deeper understanding of foot compliance and provided valuable insights for designing more efficient bio-inspired robots in the future. The proposal and investigation of this model are significant not only for fields such as biology and robotics but also provide new ideas and methods for gait control and design in engineering practice.

The next steps involve further exploration of compliant-based robot designs based on the current results, aiming to utilize compliance to achieve mobility across multiple environments. Additionally, physical experiments will also be considered in future work.

REFERENCES

[1] M. H. Raibert and J. K. Hodgins, "Animation of dynamic legged locomotion," *Proceedings of the 18th annual conference on Computer graphics and interactive techniques*, pp. 349–358, 1991.

[2] P. Ding, H. Zhao, Z. Wang, Z. Wei, S. Lyu, and D. Wang, "Quar-vla: Vision-language-action model for quadruped robots," *arXiv preprint arXiv:2312.14457*, 2023.

[3] W. Song, H. Zhao, P. Ding, C. Cui, S. Lyu, Y. Fan, and D. Wang, "Germ: A generalist robotic model with mixture-of-experts for quadruped robot," *ArXiv*, vol. abs/2403.13358, 2024. [Online]. Available: https://api.semanticscholar.org/CorpusID:268536876

[4] P. Holmes, R. J. Full, D. Koditschek, and J. Guckenheimer, "The dynamics of legged locomotion: Models, analyses, and challenges," *SIAM review*, vol. 48, no. 2, pp. 207–304, 2006.

[5] D. L. Gebo, "Foot morphology and locomotor adaptation in eocene primates," *Folia Primatologica*, vol. 50, no. 1-2, pp. 3–41, 1988.

[6] R. D. Beer, R. D. Quinn, H. J. Chiel, and R. E. Ritzmann, "Biologically inspired approaches to robotics: What can we learn from insects?" *Communications of the ACM*, vol. 40, no. 3, pp. 30–38, 1997.

[7] R. Ham, T. Sugar, B. Vanderborght, K. Hollander, and D. Lefeber, "Compliant actuator designs," *IEEE Robotics & Automation Magazine*, vol. 3, no. 16, pp. 81–94, 2009.

[8] A. Seyfarth, F. Iida, R. Tausch, M. Stelzer, O. von Stryk, and A. Karguth, "Towards bipedal jogging as a natural result of optimizing walking speed for passively compliant three-segmented legs," *The International Journal of Robotics Research*, vol. 28, no. 2, pp. 257–265, 2009.

[9] X. Xiao, O. Ma, and F. Asano, "Control walking speed by approximate-kinetic-model-based self-adaptive control on underactuated compass-like bipedal walker," *2017 IEEE International Conference on Robotics and Automation (ICRA)*, pp. 4729–4734, 2017.

[10] W. E. Harcourt-Smith and L. C. Aiello, "Fossils, feet and the evolution of human bipedal locomotion," *Journal of anatomy*, vol. 204, no. 5, pp. 403–416, 2004.

[11] L. Li, S. He, Q. Qi, J. Zeng, S. Kang, G. Endo, H. Nabae, S. Ma, and K. Suzumori, "Pegrip: A plant-tendril-inspired passive entanglement gripper enabling fail-safe grasping," *IEEE Robotics and Automation Letters*, vol. 9, no. 8, pp. 7039–7046, 2024.

[12] K. Autumn, Y. A. Liang, S. T. Hsieh, W. Zesch, W. P. Chan, T. W. Kenny, R. Fearing, and R. J. Full, "Adhesive force of a single gecko foot-hair," *Nature*, vol. 405, no. 6787, pp. 681–685, 2000.

[13] M. Sunquist and F. Sunquist, *Wild cats of the world*. University of chicago press, 2017.

[14] K. Shamaei, P. C. Napolitano, and A. M. Dollar, "Design and functional evaluation of a quasi-passive compliant stance control knee–ankle–foot orthosis," *IEEE transactions on neural systems and rehabilitation engineering*, vol. 22, no. 2, pp. 258–268, 2014.

[15] G. Chen, P. Qi, Z. Guo, and H. Yu, "Mechanical design and evaluation of a compact portable knee–ankle–foot robot for gait rehabilitation," *Mechanism and Machine Theory*, vol. 103, pp. 51–64, 2016.

[16] D. E. Lieberman, M. Venkadesan, W. A. Werbel, A. I. Daoud, S. D'andrea, I. S. Davis, R. O. Mang'Eni, and Y. Pitsiladis, "Foot strike patterns and collision forces in habitually barefoot versus shod runners," *Nature*, vol. 463, no. 7280, pp. 531–535, 2010.

[17] M. J. Coleman, A. Chatterjee, and A. Ruina, "Motions of a rimless spoked wheel: a simple three-dimensional system with impacts," *Dynamics and stability of systems*, vol. 12, no. 3, pp. 139–159, 1997.

[18] F. Asano and Z.-W. Luo, "Asymptotically stable biped gait generation based on stability principle of rimless wheel," *Robotica*, vol. 27, no. 6, pp. 949–958, 2009.

[19] T. McGeer, "Passive dynamic walking," *The International Journal of robotics research*, vol. 9, no. 2, pp. 62–82, 1990.

[20] M. Kwan and M. Hubbard, "Optimal foot shape for a passive dynamic biped," *Journal of theoretical biology*, vol. 248, no. 2, pp. 331–339, 2007.